Kinetics and Branching for the Reactions of N2+ with C3H4 Isomers at Low Temperatures and Implications for Titan's Atmosphere

Ahmad Mortada, Sophie Carles, S. Demes, Baptiste Joalland, François Lique, Abdessamad Benidar, Panayotis Lavvas, Ludovic Biennier

Kinetics and Branching for the Reactions of N_2^+ with C_3H_4 Isomers at Low Temperatures and Implications for Titan's Atmosphere

Ahmad Mortada[1], Sophie Carles[1], Sándor Demes[1], Baptiste Joalland[1], François Lique[1], Abdessamad Benidar[1], Panayotis Lavvas[2], Ludovic Biennier[1]*

[1]Univ Rennes, CNRS, IPR (Institut de Physique de Rennes) – UMR 6251, F-35000 Rennes, France

[2]Groupe de Spectrométrie Moléculaire et Atmosphérique UMR CNRS 7331, Université de Reims Champagne-Ardenne, 51687 Reims, France.

KEYWORDS: reactive collisions, uniform supersonic flows, temperature-dependent reactivity, planetary sciences, astrochemistry.

* Corresponding author: ludovic.biennier@univ-rennes1.fr

TOC GRAPHIC

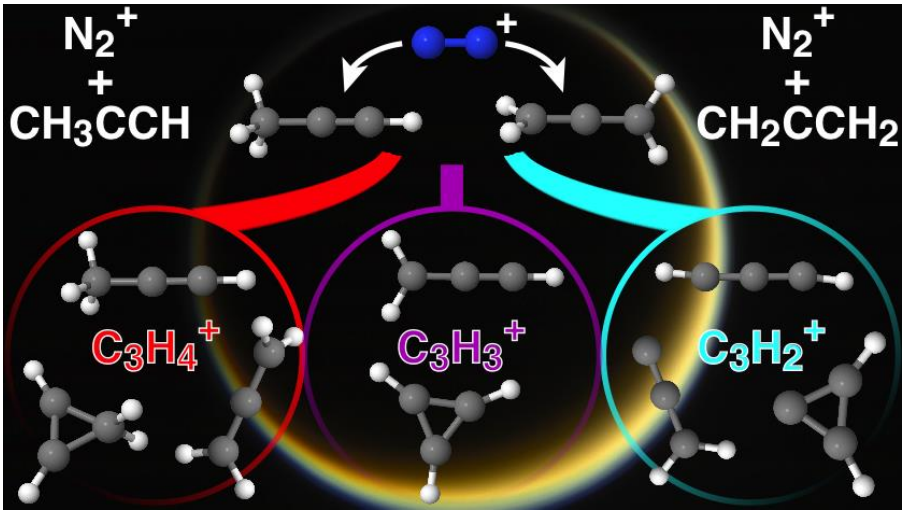

ABSTRACT

The photoionization of N_2 plays a key role in initiating the formation of complex organic molecules in the nitrogen-rich atmosphere of Saturn's largest moon, Titan. To date, only a handful of laboratory studies have explored the reactivity of N_2^+ ions with hydrocarbons—limited to methane, acetylene, and ethylene— at the low temperatures relevant to Titan. Here, the rate coefficients, product identity, and branching ratios of the ion-molecule reactions of N_2^+ with C_3H_4 isomers, namely propyne CH_3CCH and allene CH_2CCH_2, were measured between 24 and 72 K in uniform supersonic flows. The rate coefficients are collisional and their temperature-dependence is in remarkable agreement with capture models. The outcomes of both reactions are similar: they proceed primarily via dissociative charge transfer, leading to the formation of $C_3H_3^+$ (main product, >70%) and $C_3H_2^+$ (between 9 and 17%), whereas a second, nondissociative charge transfer mechanism leading to $C_3H_4^+$ becomes slightly more prominent as the temperature decreases (from 3% to 12%). $C_3H_3^+$ is plausibly formed predominantly as the smallest aromatic cation, cyclopropenyl *c*-$C_3H_3^+$, by following the lowest energy pathway for the decomposition of allene and propyne cations. The measured rate coefficients and branching ratios were included in a photochemical model of Titan's atmosphere. The results point toward a secondary role of the $N_2^+ + C_3H_4$ reactive pathways in the production of *c*-$C_3H_3^+$.

I. INTRODUCTION

The Cassini–Huygens mission to Titan, which explored Saturn's largest moon from 2004 to 2017, has revealed a fascinating and complex world that could provide a good analogue of Earth during its early history. Under irradiation from UV solar photons, bombardment from galactic cosmic rays and high energetic electrons from Saturn's magnetosphere, the dense atmosphere of Titan, dominated by nitrogen N_2 and methane CH_4, leads to the production of a wealth of organic species. Our knowledge of the atomic and molecular constituents of Titan's atmosphere, their spatial distribution and their temporal variations has also seen some significant progress through combined Earth-based and space-based observations and *in situ* measurements. The composition of the dense troposphere has been

determined by the Cassini Gas Chromatography/Mass Spectrometer (GCMS) measurements.[1] For the stratosphere, advances have relied on ground-based mm-wave instruments (IRAM, ALMA,…) [2,3] , IR space observatories ISO[4] and Herschel[5], and the Composite Infrared Spectrometer (CIRS) embarked onboard Cassini [6]. The mesosphere has been characterized by the Cassini Visible Infrared Mapping Spectrometer (VIMS)[7] and Ultraviolet Imaging Spectrograph (UVIS)[8]. The much dilute high layer of the atmosphere, the thermosphere, has been investigated by the Ion Neutral Mass Spectrometer (INMS), which conducted mass spectrometric measurements of both ions and neutrals onboard Cassini.[9] In this particular region, a plethora of hydrocarbons (two-carbon acetylene C_2H_2, ethylene C_2H_4, and ethane C_2H_6, the three-carbon propyne/allene C_3H_4, propene C_3H_6 and propane C_3H_8, the four-carbon diacetylene C_4H_2 and the six-carbon benzene C_6H_6) and nitriles (hydrogen cyanide HCN and hydrogen isocyanide HNC, cyanoacetylene HC_3N, acetonitrile CH_3CN, acrylonitrile CH_3CCN, propanenitrile C_2H_5CN, cyanogen C_2N_2) have been detected.

The INMS mass spectra spanning the 0-100 u range show peaks arranged in clusters separated by 10 to 15 u that coincide with the sequential addition of hydrogenated carbon or nitrogen atoms. Noteworthy, a good correspondence is found between the ion and neutral spectra. However, due to the low resolution of the embarked mass spectrometer ($m/\Delta m$~100), and the absence of isomer identification inherent to the method, the assignment of the peaks cannot be self-sufficient and relies heavily on a good knowledge of the chemistry. The latest modeling study based on INMS measurements[9] puts forward key hydrocarbon ions such as CH_3^+, CH_5^+, $C_2H_5^+$, $C_3H_3^+$, $C_3H_5^+$, $C_4H_3^+$, $C_4H_5^+$, $C_6H_7^+$, $C_7H_7^+$, and nitriles such as $HCNH^+$.[10] Many other ions stay under the radar because of mass overlap; they include N_2^+ since $HCNH^+$ is the dominant species at m/z=28 u, and also N_2H^+ concealed by $C_2H_5^+$ (m/z=29 u). To assess their presence, well-known reactions dominating their loss processes can be employed. The best tracer of N_2^+ is considered to be CH_3^+ as it can only be produced massively through the reaction of N_2^+ with the second most abundant species in the atmosphere, methane CH_4.[11,12] The N_2^+ cation is of particular importance as it is considered as a primary ion - i.e. generated in the early stages of the chemical network - along with N^+ and CH_4^+. These three cations

are directly produced upon interaction of N_2 and CH_4 with solar photons and suprathermal photo- and secondary electrons.

Propyne CH_3CCH has been first uncovered in the Voyager IR spectrum of Titan in the 80's. A stratospheric abundance of CH_3CCH of 3×10^{-8} was determined for the mid-latitude region.[13] Further observations by ISO in 2003 led by Coustenis[4] provided a disk average value of 1.2×10^{-8}. During targeted flybys [14,15], Cassini/INMS measured the abundance of propyne in the ionosphere and derived a mole fraction in the $2–7\times10^{-6}$ range. Propyne was also detected by the CIRS instrument[16] through its 633 cm^{-1} emission feature and through infrared observations made with the Texas Echelle Cross Echelle Spectrograph (TEXES) on the NASA Infrared Telescope Facility.[17] Propadiene, also referred to as allene, CH_2CCH_2, an isomer of propyne, was unambiguously identified by TEXES observations through its emission near 12 μm with a measured volume mixing ratio of 6.9×10^{-10} at the altitude of 175 km. CIRS measurements of propyne made at the same time indicate that the abundance ratio of propyne to propadiene is 8.2 at the same altitude. Propyne and propadiene constitute the first hydrocarbon isomer pair detected on Titan. Both isomers have been included in several photochemical models.[10,18] According to Dobrijevic et al.,[19] the main pathway for the formation of both isomers in the stratosphere is the associative reaction between hydrogen and propargyl radicals (C_3H_3):

$$C_3H_3 + H\ (+M) \rightarrow C_3H_4\ (+M) \qquad (1)$$

Below 200 km, the CH_2CCH_2 molecule can be produced additionally by the photodissociation of propene (C_3H_6).

In the ionosphere, C_3H_4 can be generated through the reaction of the CH radical with C_2H_4 and through the recombination of $C_3H_5^+$ with electrons:

$$C_3H_5^+ + e^- \rightarrow C_3H_4 + H \qquad (2)$$

The primary loss channel of C_3H_4 is the photodissociation leading to propargyl C_3H_3:

$$C_3H_4 + h\nu \rightarrow C_3H_3 + H \qquad (3)$$

Conversion from propadiene to propyne can take place through the reaction:

$H + CH_2CCH_2 \rightarrow CH_3CCH + H$ (4)

The ion and neutral chemistry proposed above is however incomplete as major sources of uncertainty remain, besides the fact mentioned above that the INMS measurements cannot alone rule out isomers and lead to a firm identification of the alleged species. In particular, major sources of uncertainty come from the lack of information on product identity and branching as well as their temperature dependence (available data are often restricted to room temperature). While this is especially problematic for radical-neutral reactions, with only one study below 50 K reported so far[20], several techniques have been developed to measure the low-temperature kinetic rate coefficient and/or the products of ion-molecule reactions: crossed and merged molecular beams, ion traps and flow reactors. Cryogenic ion traps are for instance tailored to examine the reaction kinetics of ions over a wide dynamic range.[21] In practice however, condensation of the neutral co-reactants onto the walls of the chamber limits their use to light neutrals such as H_2 or He.[22] Uniform supersonic flows, which belong to the family of flow reactors, are well adapted to explore quantitatively the reactivity of ions with large neutral molecules[23–25] – it is one of the rare techniques to provide rate coefficients obtained under well-controlled thermalized conditions and over a wide range of low temperatures[26]. Here, a new approach combining a CRESU (Cinétique de Réaction en Ecoulement Supersonique Uniforme) reactor with a mass-selective ion source[27] was used to measure for the first time the low-temperature rate coefficients and product branchings of two key Titan's atmospheric reactions involving isomeric hydrocarbon targets: N_2^+ with propyne CH_3CCH and allene (propadiene) CH_2CCH_2 at 24, 36, 49, 57, and 71.6 K.

II. EXPERIMENTAL METHODS

The low-temperature reactions of N_2^+ with C_3H_4 isomers were investigated using a novel mass selective ion source (SIS) combined with a CRESU flow reactor. The experimental setup allows for measuring the absolute rate coefficient and the branching ratios of targeted gas-phase reactions at various low temperatures (down to 15 K). Details on this new approach can be found in previous work[27] and are only briefly summarized hereafter. The neutral cold and dense uniform supersonic flow

is generated by the isentropic expansion of a continuous buffer gas (here helium or a mixture of helium and nitrogen) through a de Laval nozzle. The density, velocity and temperature in the core of the supersonic flow are uniform over several tens of centimetres (See Table 1 for the characteristics of the de Laval nozzles used in this work). The buffer gas flow can reach 100 slm (standard liter per minute) thus requiring substantial pumping capacity (up to 35 000 m^3/h) to maintain a low pressure (typically 0.1 mbar) in the main chamber. The high density of the flow (about 10^{16} molecule cm^{-3}) ensures local thermodynamic equilibrium and rapid rotational relaxation of the molecular species (charged or neutral). The supersonic flow, which can be viewed as a wall-less chemical reactor, was inseminated with a small quantity of the studied ionic and neutral reactants allowing reactive collisions. The neutral reactants propyne and allene (Air Liquide, 96% and 98% purity, respectively) were injected continuously in the supersonic flow with a flow rate of a few sccm (standard cubic centimeter per minute) corresponding to a density of about 10^{12} molecule cm^{-3}.

N_2^+ ions were produced in a plasma generated by a hollow cathode discharge ($P \sim 2$ mbar, $U_{discharge} \approx$ 395 V, $I_{discharge} \approx 950$ mA) obtained with a continuous flow of helium (0.750 slm) and nitrogen N_2 (5 sccm). The mass selection of the N_2^+ ions was performed by a quadrupole mass filter giving an output ion current of about 1 nA. Several quadrupole and octopole ion guides are used to transport ions from their production zone, through the selection mass filter and finally down to the uniform supersonic flow with a good transmission. The ion current measured at the injection lens of the SIS was about 600 pA. In this configuration, the ions arrive at right angle compared to the neutral uniform supersonic flow axis requiring a deflector with adapted applied potentials (around +3 V and -30 V for radial and vertical axes) to inflect their trajectory. According to Kato *et al.*[28] and Ferguson[29], the collisional vibrational relaxation coefficient of $N_2^+(v=1)$ by N_2 is about $5\text{-}8\times10^{-10}$ cm^3 $molecule^{-1}$ s^{-1}, meaning that the relaxation to the ground state is achieved in a few µs, i.e. directly in the plasma of the SIS start station. As a result, the N_2^+ ions are in their ground vibrational state before being injected into the uniform supersonic flow. The ionic species (reactants and products) were detected along the uniform supersonic flow axis by a moveable detector equipped with an entrance skimmer (80 µm diameter), a hexapole ion guide, a quadrupole mass filter (0-100 u), and a Channeltron ion multiplier. Because of

the constant flow velocity, the moveable detector allows to follow the temporal evolution of the ion densities for a hydrodynamic time τ_h of typically 150-200 µs.

TABLE 1: Characteristics of the supersonic uniform flows employed in this study and determined from impact pressure measurements.

Nozzle	Buffer gas	T_{jet} (K)	Mach	τ (µs)	n (10^{16} molecule.cm^{-3})	$P_{chamber}$ (mbar)	flow rate (l/min)
He6K	He	24.1	5.84	196	18.3	0.630	93.4
He36K	He	36.1	4.63	195	5.28	0.293	84.7
Ar7K	He	49.0	3.87	150	10.4	0.770	67.0
Ar7K	He/N_2 (1:1)	57.0	4.08	158	6.91	0.550	20:20
Ar50K0.3	He	71.6	3.08	163	6.01	0.640	97.7

III. RESULTS

Reaction Products Figure 1 shows two mass spectra recorded at 49 K after a reaction time of t = 50 µs and with a reactant density [C_3H_4] = 1.4×10^{12} molecule cm^{-3} for propyne and allene. For both reactions, the main ion product detected is $C_3H_3^+$, followed by $C_3H_2^+$ and $C_3H_4^+$ ions (respectively *m/z*=39, 38 and 40 u). In addition, the mass spectra reveal traces of $C_3H_5^+$ (*m/z*=41 u) and C_3H^+ (*m/z*=37 u) as can be seen on the inset of Figure 1. Without any neutral reactant, ions other than N_2^+, namely N_2H^+ at *m/z* = 29 u, NO^+ at *m/z* = 30 u, O_2^+ at *m/z* = 32 u, H_2O^+ at *m/z*= 18 u, and H_3O^+ at *m/z*= 19 u, are also detected.

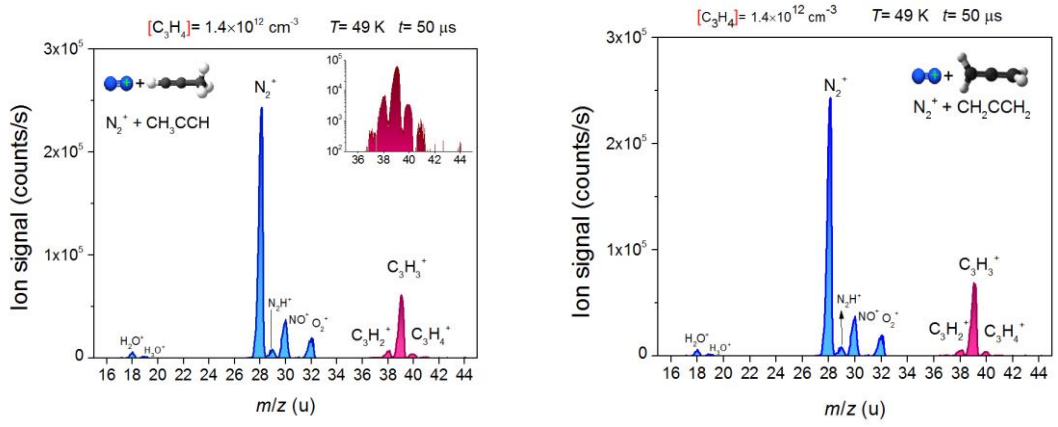

FIG 1: Mass spectra measured in a 49 K uniform supersonic flow inseminated by mass-selected N_2^+ cations in presence of CH_3CCH (A) and CH_2CCH_2 (B) neutral reactants at a density of 1.4

$\times 10^{12}$ molecule cm^{-3}. The ions are detected at a distance of 8 cm from the injection lens of the SIS, corresponding to a reaction time of 50 µs. The inset shows a close-up of the products in log scale.

These ions are the products of reactions of N_2^+ with impurities present in the neutral supersonic flow, unless they are not filtered out by the SIS due to the large bandpass of our quadrupole mass filter ($\Delta m/z = \pm 4$ u). The reactions with impurities are considered as follows:

i. The H_3O^+ + C_3H_4 (propyne and allene) reactions have been studied in SIFT (Selected Ion Flow Tube) and FA-SIFDT (Flowing Afterglow - Selected Ion Flow Drift Tube) experiments at room temperature and the only observed exit channel for both reactions is $C_3H_5^+$ + H_2O with reaction enthalpies ΔH = -0.83 and -0.87 eV and rate coefficients k = 1.7-1.8 and 1.4×10^{-9} cm^3 $molecule^{-1}$ s^{-1} for propyne and allene, respectively.[30,31]

ii. The H_2O^+ + C_3H_4 reaction is considered as a source of $C_3H_5^+$ and potentially $C_3H_4^+$ in line with the proton affinities of propyne (748 kJ/mol) and allene (775.3 kJ/mol) which are larger than the ones of OH (593.2 kJ/mol) and H_2O (691 kJ/mol).[32] The contribution of the H_2O^+ + C_3H_4 reaction to the BR of $C_3H_4^+$ is weak. As an illustration, the H_2O^+ ion signal drops by less than 5 % in the presence of neutral reactant with a density [C_3H_4] of 6×10^{12} molecule cm^{-3}, meaning that H_2O^+ is not highly reactive with C_3H_4. In spite of its small contribution, this effect is taken into account in the determination of the branching ratios of the N_2^+ + C_3H_4 reactions.

iii. According to Milligan *et al.*, N_2H^+ reacts with C_3H_4 to form the $C_3H_5^+$ ion exclusively as it has been observed in FA-SIFDT experiments at 300 K [31]. The experimental rate coefficients are k = 1.5 and 1.4×10^{-9} cm^3 $molecule^{-1}$ s^{-1} and the corresponding reaction enthalpies are ΔH = -2.87 and -2.91 eV for propyne and allene, respectively.

iv. The NO^+ + C_3H_4 (propyne and allene) reactions have also been studied in SIFT experiments[30] at 298 K. Propyne only generates the $[C_3H_4{\cdot}NO]^+$ adduct with a rate coefficient of $k = 6.3\times10^{-11}$ cm^3 $molecule^{-1}$ s^{-1}, while the reaction with allene exhibits two exit channels corresponding to the $[C_3H_4{\cdot}NO]^+$ adduct (90%) and the $C_3H_3^+$ ion (10%). However, the rate coefficient $k = 2.5\times10^{-11}$ cm^3 $molecule^{-1}$ s^{-1} for the NO^+ + CH_2CCH_2 reaction is too low to be competitive here. The lack of a

significant drop in the NO^+ signal at low temperatures (a few percent) and the absence of an ion signal at *m/z*=70 u allow to discard any interference from the $NO^+ + C_3H_4$ reactions.

v. Two SIFT experiments have been performed at room temperature to examine the $O_2^+ + C_3H_4$ (propyne and allene) reactions. Wilson *et al.* only observed the charge transfer reaction, i.e. $C_3H_4^+ + O_2$, with rate coefficients of k = 1.6 and 1.3×10^{-9} cm^3 $molecule^{-1}$ s^{-1} for propyne and allene respectively [30]. Dicker *et al.*, also studied the $O_2^+ + CH_2CCH_2$ reaction and derived a rate coefficient $k = 1.3\times10^{-9}$ cm^3 $molecule^{-1}$ s^{-1}, but they observed three exit pathways: the charge transfer (94%), the $C_3H_3^+ + HO_2$ exit channel (4%) and the $CH_2CO^+ + CH_2O$ one (2%) with calculated corresponding enthalpies ΔH = -2.39, -2.87 and -2.91 eV [34]. In the work of Wilson *et al.*[30], the presence of vibrationally excited O_2^+ ions was assumed. In the latter experiments of Decker *et al.*[34], this issue was considered and O_2 was added to quench the excited O_2^+ ions. This can explain the different results from the two SIFT experiments. Then, the $C_3H_4^+$ and $C_3H_3^+$ ions can also be formed by the $O_2^+ + C_3H_4$ reaction, this is considered in the branching ratio determination (see thereafter).

vi. For the C_3H^+ product, all the reaction enthalpies calculated in this work for the different exit channels of the $N_2^+ + C_3H_4$ reactions are positive (see Figure 2), suggesting that the observed C_3H^+ traces come from a secondary reaction between C_3H_4 and some impurities. These reactions do not affect the evolution of the N_2^+ density and therefore the derived rate coefficient of the studied reactions.

In order to qualitatively analyze the stoichiometry of the species observed in the mass spectra we performed a reduced theoretical analysis by calculating the enthalpies of formation and the corresponding relative reaction enthalpies by means of high level *ab initio* theories. The *ab initio* calculations were performed using the spin unrestricted coupled-cluster theory with single and double excitations (UCCSD) along with the augmented correlation-consistent valence double zeta (aug-cc-pVDZ) basis set. All calculations were carried out with the MOLPRO (version 2015.1) quantum chemistry software package[35,36]. The structure and energy properties of all molecular species were determined in their minimum configuration, i.e. following full geometry optimization. Various starting geometries were examined in order to find the structures and properties of the most stable $[N_2–C_3H_4]^+$

complexes. Harmonic vibrational frequency and normal mode calculations were performed to compute the zero-point vibrational energies (ZPVE) and the total enthalpies of formation. More details about the geometries and energies of the species are given in the Supplementary Material.

Figure 2 shows the schematic diagram of the relative reaction enthalpies for the observed hydrocarbon cations and a few other related ones. Since the experiments were carried out at various temperatures, the reaction enthalpies were calculated at 0 K only, i.e. taking into account the total electronic and zero point vibrational energies exclusively. Note that many more cyclic complexes exist but our analysis was limited to the two most stable $[N_2C_3H_4]^+$ ones.

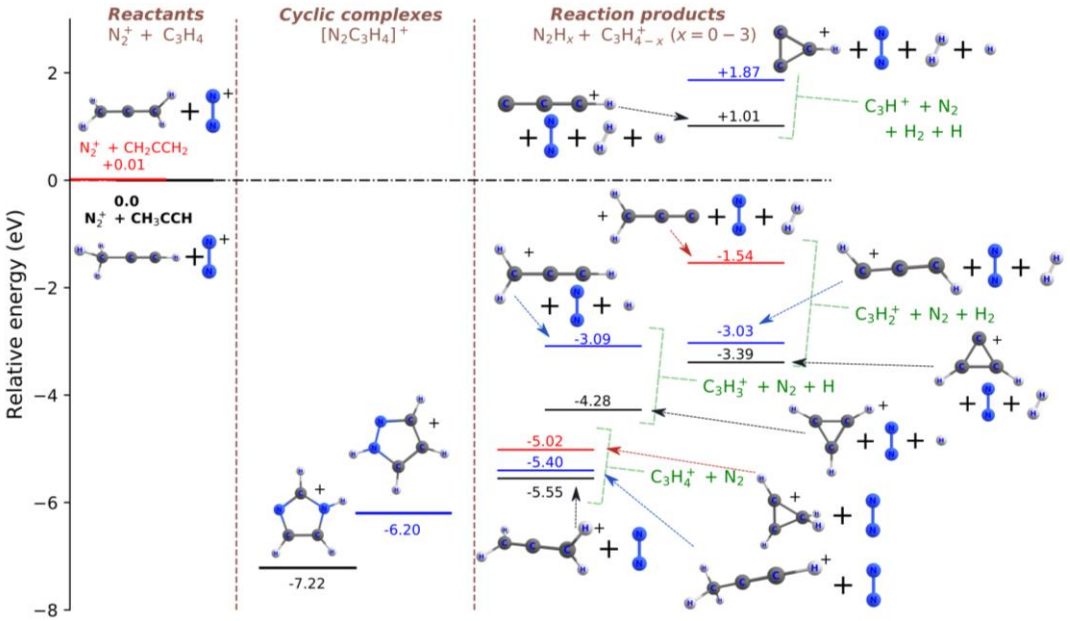

FIG 2: Schematic diagram of the $N_2^+ + CH_3CCH$ and $N_2^+ + CH_2CCH_2$ reaction enthalpies with the experimentally observed (or potential) formation channels of $C_3H_{4-x}^+$ ($x = 0–3$) ion products. The enthalpy of all species is calculated in the UCCSD/aug-cc-pVDZ framework, including ZPVE corrections. All energies are relative to separated N_2^+ and propyne (CH_3CCH) reactants.

Given the low temperatures of the experiments, the $N_2^+ + C_3H_4$ reactions can only form exoergic products i.e. $CH_2CCH_2^+$ and CH_3CCH^+ cations (pure charge transfer) as well as the different $C_3H_3^+$ and $C_3H_2^+$ isomers. According to our calculations the endoergic exit channels towards the C_3H^+ cations remain out of reach. As one can also see in Figure 2, the most exoergic $N_2C_3H_4^+$ species have a cyclic structure. The first of them (1H-imidazole cation) has a very large relative exoergicity of about -

7.22 eV, while the second isomer (pyrazole cation) has a slightly higher relative enthalpy, with about -6.20 eV. Both of these cations are highly exoergic with respect to the reactants and the $C_3H_4^+$, $C_3H_3^+$ and $C_3H_2^+$ product formation channels. However, since the formation of these cyclic species implies strong re-orientations and multiple internuclear rearrangements which possibly involve many intermediate transition states, we expect that such $N_2C_3H_4^+$ complexes do not form effectively from the linear molecular reactants.

Charge transfer reactions (both dissociative and nondissociative), which lead to the formation of the observed $C_3H_4^+$, $C_3H_3^+$ and $C_3H_2^+$ products, most probably proceed via the formation of non-stable, quasi-bound complexes (i.e. complex with large intramolecular distance, in agreement with the capture theory), producing excited $C_3H_4^+$ cations preliminarily. These complexes are represented by close superposition of the colliding molecular species, where their bond lengths and angles are not distorted, but where the electron exchange from C_3H_4 towards N_2^+can effectively proceed, involving electronic transitions between multiple potential energy surfaces. This mechanism is supported by the Franck-Condon principle, according to which the electronic transitions proceed much faster than nuclear movements and rearrangements. If the primary cations are formed by conserving a large amount of internal energy, their dissociation proceeds according to a unimolecular decomposition scheme.

Rate coefficients. Kinetic data were obtained under pseudo-first order conditions, i.e. with a [C_3H_4] neutral density in excess compared to the [N_2^+] density. The loss rate of N_2^+ was determined by the evolution of the N_2^+ signal with time for a given neutral reactant density. The variation of the N_2^+ loss rates with the neutral reactant density gives the absolute rate coefficient *k(T)* of the reaction at a fixed temperature, as illustrated in Figure 3 for N_2^+ + CH_2CCH_2 at 24 K. The results are summarized in Table 2.

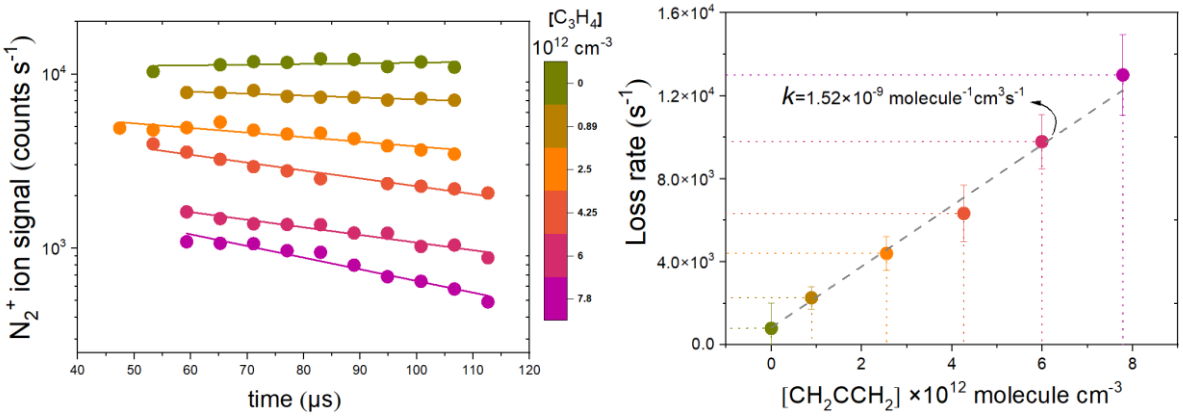

FIG 3: N_2^+ ion signal as a function of time for a range of neutral CH_2CCH_2 densities (left) and corresponding loss rates as a function of CH_2CCH_2 densities (right) at 24 K.

TABLE 2: Absolute rate coefficients k of the N_2^+ + CH_3CCH and N_2^+ + CH_2CCH_2 reactions measured with the CRESU-SIS device at different temperatures in $\times 10^{-9}$ cm^3 molecule^{-1} s^{-1} unit. The uncertainties take into account statistical and systematic (10%) contributions.

T (K)	24.1	36.1	49.1	57.0	71.6
N_2^+ + CH_3CCH	3.73 ± 0.41	3.4 ± 0.36	2.52 ± 0.34	2.39 ± 0.25	2.13 ± 0.21
N_2^+ + CH_2CCH_2	1.52 ±0.16		1.40 ±0.2		1.56 ±0.22

For N_2^+ + CH_2CCH_2, the rate coefficients show a quasi-independence with temperature. The measured values are in good agreement with the Langevin value of k_L=1.38×10^{-9} cm^3 molecule^{-1} s^{-1} estimated from $k_L = 2\pi e\sqrt{\alpha/\mu}$, where e is the elementary charge, α the static dipole polarizability of the neutral molecule ($\alpha_{CH2CCH2}$= 5.69 Å^3 from Ref. [37]), and μ the reduced mass of ion-molecule system. For N_2^+ + CH_3CCH, the Langevin model is not suitable since the permanent dipole moment μ_D of the neutral reactant is not considered. For a polar neutral reactant, the Su and Chesnavich model[38] gives a rate coefficient $k_{SC} = K_{cap} \times k_L$ which is temperature dependent with $K_{cap} = 0.4767x + 0.6200$ when $x = \frac{\mu D}{\sqrt{2\alpha T k_B}} \geq 2$. Considering the dipole moment of propyne (μ_D=0.784 D)[39] and its polarizability (α_{CH3CCH}= 5.55 Å^3)[40], we determined for all the temperatures a value of the x parameter greater than 2 for the studied N_2^+ + CH_3CCH reaction. Then the estimated values of the rate coefficients from the Su and Chesnavich model are k_{SC}=3.49, 3.01, 2.70, and 2.38×10^{-9} cm^3 molecule^{-1} s^{-1} at 24, 36, 49, and

71.6 K respectively. Figure 4, which displays the experimental values obtained in this work and the estimated values obtained from the simple capture models of Langevin and Su and Chesnavich, illustrates their remarkable agreement.

Several arguments concur to rule out termolecular processes for the $N_2^+ + C_3H_4$ reactions. First, no peak at *m/z*= 68 u, corresponding to the association product, is detected in the mass spectra. Second, the rate coefficient of the N_2^+ with CH_3CCH reaction is not affected by changing the buffer gas, *i.e.* pure helium at 49.1 K and helium-nitrogen mixture (1:1) at 57 K. Thirdly, an increase of the total density or a decrease of the temperature both lead to a rise of the rate coefficient in a termolecular process; yet the measured rate coefficients for propyne and allene follow closely the Su and Chesnavich and the Langevin models, respectively (see Figure 4), including between 24.1 K and 36.1 K where the total density is changed by more than 3-fold (18.3×10^{16} and 5.28×10^{16} molecule cm^{-3}, respectively). This set of observations strongly supports a bimolecular process only.

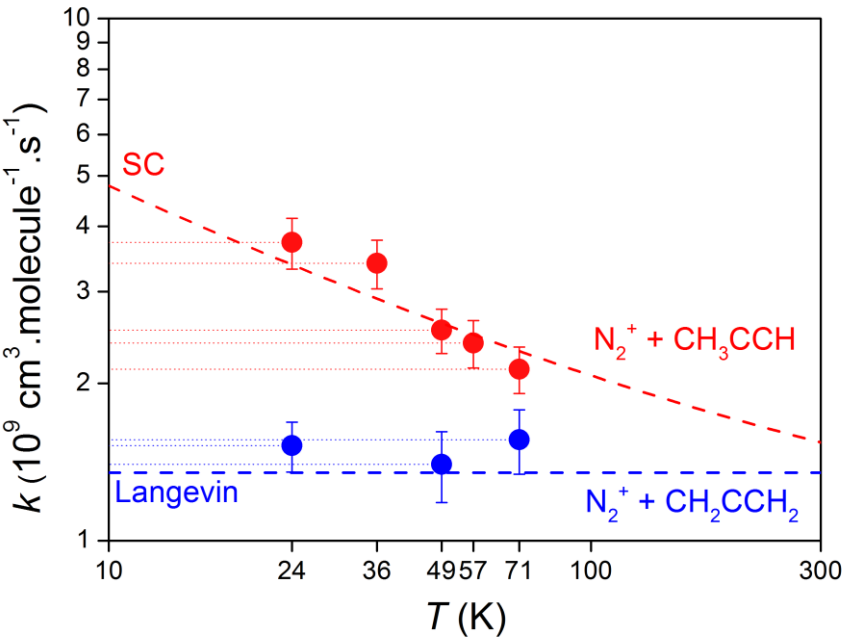

FIG 4: Comparison between the measured absolute rate coefficients *k* as a function of temperature for the N_2^+ with CH_3CCH (red filled circles) and CH_2CCH_2 (blue filled circles) reactions and the Langevin (blue dashed line) and Su & Chesnavich (red dashed line) models.

Branching ratios The $C_3H_2^+$, $C_3H_3^+$ and $C_3H_4^+$ ions are clearly identified as the primary products of the N_2^+ + CH_3CCH / CH_2CCH_2 reactions. The enthalpies of the N_2^+ + C_3H_4 reactions producing C_3H^+ are positive and the formation of $C_3H_5^+$ is well explained by the reactions between N_2^+ with impurities. As mentioned above as well, the O_2^+ + C_3H_4 reaction represents however a small but non-negligible source (up to a few percent) of $C_3H_3^+$ and $C_3H_4^+$ ions, even if the initial abundance of N_2^+ ions is much higher—by a factor of 16—than the abundance of O_2^+. In order to determine accurate branching ratios for the N_2^+ + C_3H_4 reactions, we have also explored the low-temperature reactivity of O_2^+ with propyne and allene with our CRESU-SIS experimental setup—the results will be presented in detail in an upcoming publication. In this case, the detected products are $C_3H_3^+$, $C_3H_4^+$, and $C_2H_2O^+$ (with branching ratios $\alpha(T)$, $\beta(T)$, and $\chi(T)$, respectively), in agreement with Decker *et al.*'s observations for allene at 300 K. The small contributions of the O_2^+ + C_3H_4 reactions measured while studying the N_2^+ + CH_3CCH / CH_2CCH_2 reactions were eliminated by subtracting $\alpha(T)\times\Delta O_2^+$ and $\beta(T)\times\Delta O_2^+$ to each of the $C_3H_3^+$ and $C_3H_4^+$ integrated peaks, respectively, with ΔO_2^+ representing the decrease of the O_2^+ ion signal.

The apparent BRs for the three exit channels $C_3H_2^+$, $C_3H_3^+$ and $C_3H_4^+$, corrected to eliminate the contributions of the O_2^+ + C_3H_4 reactions, are shown in Figure 5 as a function of [C_3H_4] density in the case of propyne at 49 K. The values vary slightly and linearly with the [C_3H_4] density, due to secondary reactions of the primary ion products with C_3H_4. To limit the contribution of those reactions, the BRs were determined at short reaction times and by extrapolating their values for a null [C_3H_4] density = 0 (*y*-intercept of the linear fit).

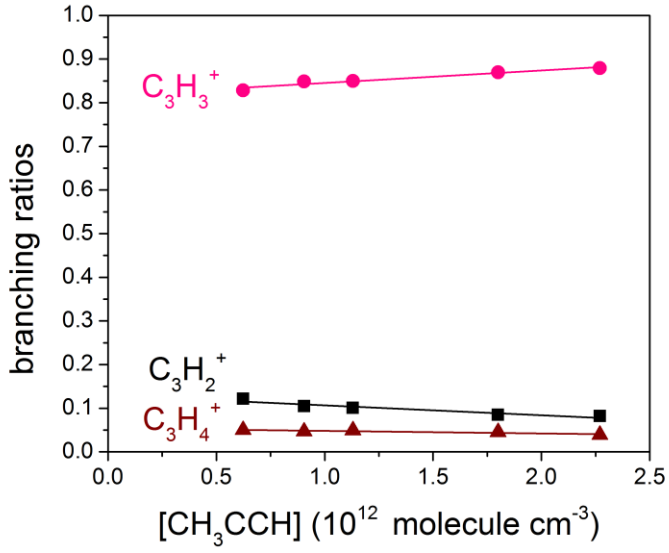

FIG 5: Evolution of the branching ratios (BRs) with the [CH_3CCH] density, measured at 49 K for a reaction time of 56 μs. The BRs are corrected to eliminate the contribution of the $O_2^+ + C_3H_4$ reaction.

The BRs of the studied reactions and their temperature dependence, obtained after correction for the $O_2^+ + C_3H_4$ reaction contributions and extrapolation to a null [C_3H_4] density, are shown in Figure 6 and summarized in Table 4. For both reactions, the BR of the main exit channel leading to $C_3H_3^+$ decreases as the temperature decreases, while no significant variation is observed for the other dissociative $C_3H_2^+$ exit channel. Hence, a small yet significant increase of the BR associated with the nondissociative charge transfer reaction leading to $C_3H_4^+$ is observed.

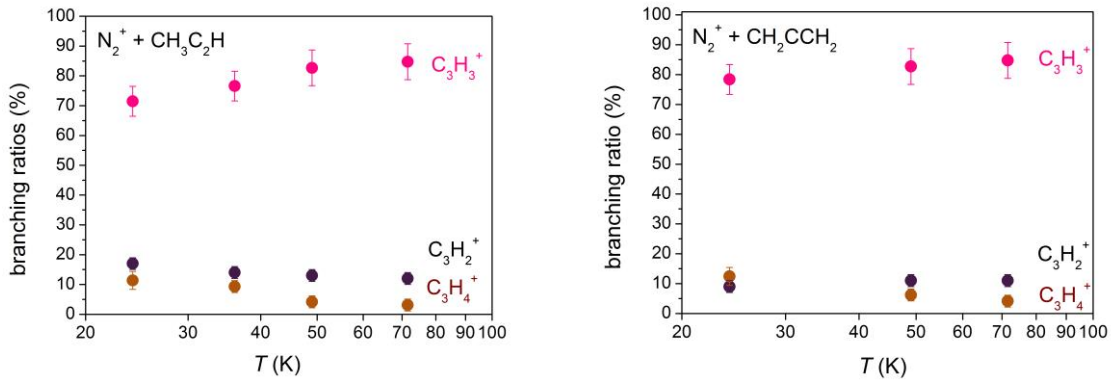

FIG 6: Temperature dependence of the branching ratios between the primary products of $N_2^+ + CH_3CCH$ (left) and $N_2^+ + CH_2CCH_2$ (right) reactions. The error bars were estimated by adding systematic (±0.02) and statistical (±5%) contributions.

TABLE 4: Branching ratios of the reactions of N_2^+ with the two C_3H_4 isomers at 24.1, 36.1, 49.0 and 71.6 K. These values take into account the natural isotopic abundance of carbon 13.

	CH_3CCH				CH_2CCH_2			
T (K)	24.1	36.1	49.0	71.6	24.1	36.1	49.0	71.6
$C_3H_2^+$	0.17	0.14	0.13	0.12	0.09	-	0.11	0.11
$C_3H_3^+$	0.72	0.77	0.83	0.85	0.785	-	0.83	0.85
$C_3H_4^+$	0.11	0.09	0.04	0.03	0.125	-	0.06	0.04

IV. DISCUSSION

Reaction dynamics To better understand the outcomes of the title reactions, we first invoke the reaction of Ar^+ with ethylene C_2H_4 studied in a flowing-afterglow apparatus by Tsuji *et al.* [41], as Ar^+ is only slightly more energetic than N_2^+ (recombination energy of 15.76 eV for Ar^+ versus 15.58 eV for N_2^+). The reported branching was 0.76:0.20:0.04 for $C_2H_2^+$:$C_2H_3^+$:$C_2H_4^+$. The $C_2H_2^+$:$C_2H_3^+$ ratio was found to increase further while increasing the internal energy of $C_2H_4^+$. From these measurements it was inferred that 95% of the CT excess energy is released into internal energy of the $C_2H_4^+$ ion before its decomposition. The authors concluded that the reaction proceeds via two competing mechanisms:

i. A near-resonant, dissociative CT occurring at long range without significant momentum transfer. This mechanism is dominant and leads to the formation of $C_2H_2^+$ and $C_2H_3^+$. It involves nonadiabatic transitions between charge states of $N_2^+ + C_2H_4$ and $N_2 + C_2H_4^+$, which populate some of the $C_2H_4^+$ excited electronic states.

ii. A nonresonant, nondissociative CT occurring via an "intimate collision" that enables significant momentum transfer. This mechanism is responsible for the $C_2H_4^+$ product, which is formed with less internal energy when compared to dissociative CT and therefore cannot decompose.

In the case of reactions of N_2^+ with hydrocarbons, Gichuhi and Suits have measured the product branching for the reactions of N_2^+ with methane CH_4, acetylene C_2H_2, and ethylene C_2H_4 at 40 K using a modified velocity map imaging apparatus.[42] The reaction with acetylene was found to form only $C_2H_2^+$ via nondissociative CT, while the reaction products for the reaction with ethylene led to the formation of $C_2H_2^+$ and $C_2H_3^+$ whereas no $C_2H_4^+$ was observed, suggesting that this reaction proceeds only via the near-resonant dissociative mechanism. Interestingly, the branching of 0.76:0.24 is remarkably close to the one measured for the $Ar^+ + C_2H_4$ reaction.

In light of these previous results, the two CT mechanisms (dissociative and nondissociative) are likely responsible for the outcomes of the reactions studied here, although a careful mapping of the potential energy surfaces of the $N_2^+ + C_3H_4$ system would be necessary to fully validate this assumption. The measured rate coefficients, which are all collisional, indeed suggest that these fast reactions take place at long range via CT. The CT can deposit more than 5 eV of internal energy in the $C_3H_4^+$ precursor (based on the NIST Chemistry WebBook, the CT between N_2^+ and propyne releases 5.22 eV; the CT between N_2^+ and allene releases 5.89 eV). $C_3H_4^+$ can then undergo rapid internal conversion to the ground state and possibly rearrange before the cleavage of C-H bonds occurs. The potential energy diagram of $C_3H_4^+$, adapted from Mebel and Bandrauk [43], is shown in Figure 7. The lowest-energy dissociation channel leads to cyclopropenyl *c*-$C_3H_3^+$ + H, with an energy of 1.68 eV and a transition state (TS) at 1.87 eV above $CH_2CCH_2^+$, i.e. about one third of the total excess energy. This pathway implies the rearrangement of $CH_2CCH_2^+$ and CH_3CCH^+ into *c*-$C_3H_4^+$ prior dissociation. The pathway leading to *l*-$C_3H_3^+$ + H is barrierless and the exit channel lies 2.84 eV above $CH_2CCH_2^+$—about one half of the available energy. At similar energies lie the two lowest-energy H_2 loss channels, namely $CH_3CCH^+ \rightarrow HCCCH^+ + H_2$ (2.79 eV, TS at 2.93 eV), and *c*-$C_3H_4^+ \rightarrow$ *c*-$C_3H_2^+ + H_2$ (2.56 eV, no TS found). The only other exit channel energetically accessible after CT with N_2^+ is the loss of H_2 from $CH_2CCH_2^+$, (4.39 eV, no TS found) which requires more than two thirds of the excess energy to be funneled into.

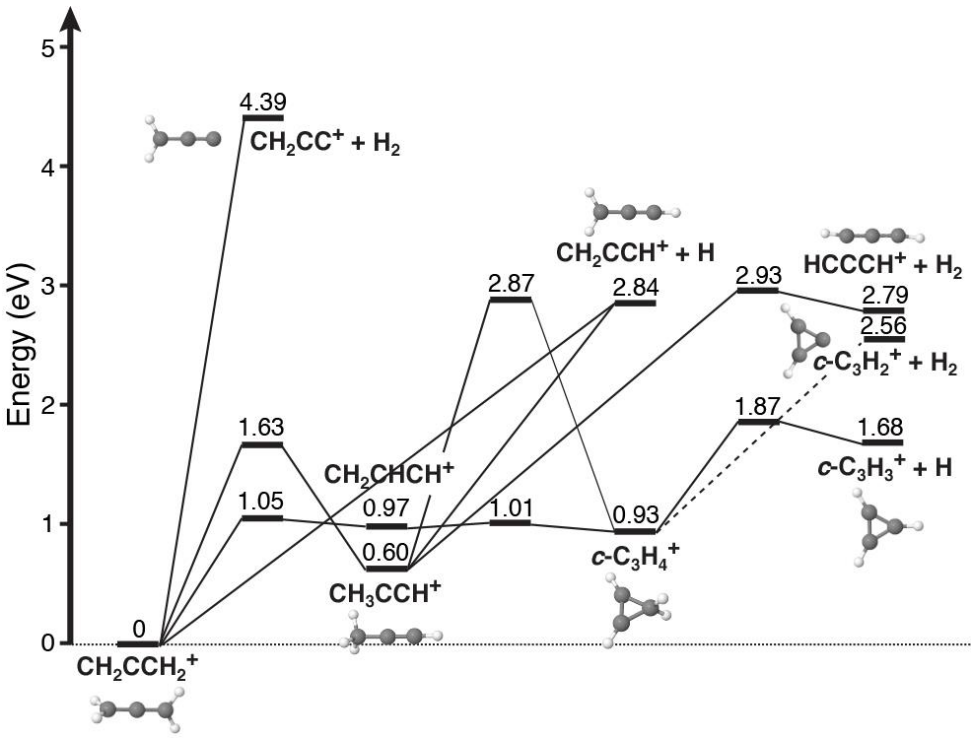

FIG 7: Potential energy diagram of the ground state of $C_3H_4^+$, adapted from Mebel and Bandrauk[43]. Energies were calculated at the CCSD(T)/cc-pVTZ//B3LYP/6-311G** level of theory and are shown relative to the global minimum, the allene cation $CH_2CCH_2^+$. All the dissociation channels accessible for the ion precursor after charge transfer with N_2^+, which can deposit up to 5.89 eV into $C_3H_4^+$, are reported. Note that no transition states were found for the H_2 loss channels from $CH_2CCH_2^+$ and *c*-$C_3H_4^+$—dashed lines connect these stationary points.

These energy considerations are fully in line with the measured branching ratios. Previous experimental work on the unimolecular decomposition of $CH_2CCH_2^+$ and CH_3CCH^+ have shown that the main isomer formed is cyclic $C_3H_3^+$,[44–46] corresponding to the lowest-energy dissociation channel on the $C_3H_4^+$ potential energy surface. Liu et al.[47] investigated theoretically the isomerization barrier to form *c*-$C_3H_3^+$ from linear propargylium H_2CCCH^+ at the QCISD(T)/6-311+G(d,p)//B3LYP/6-31G(d) level of theory. They reported a direct pathway with a 3.8 eV barrier and a pathway through TS – intermediate – TS with a 2.1 eV barrier, both well above the relative enthalpy of 1.1 eV. In case of an internally highly excited $C_3H_4^+$ cation, both cyclic and linear $C_3H_3^+$ isomers may form via unimolecular decomposition processes. The allene and propyne cations formed in electronic/vibronic excited states via CT might not necessarily dissociate following the lowest energy pathway, as e.g. pointed out in a work on the photoabsorption and photoionization of propyne[46]. The examination of

unimolecular decomposition process which has guided part of our analysis so far may provide some further hints. In the absence of quantitative determination of branching ratios between isomers from photoionization, one can turn to electron-impact ionization studies. Infrared spectroscopic measurements conducted by Brünken *et al.*[48] showed that electron-impact ionization of allene CH_2CCH_2 leads to the dominant production of the cyclic $C_3H_3^+$ isomer (81%) over the linear one (19%) and that the isomeric ratio is independent of the electron energy over the 14-70 eV range. Only a fraction of the energy of the colliding electron will effectively contribute to ionize and excite the molecule as most of it will be carried away with the electron itself after the encounter, since elastic electron scattering cross sections are typically orders of magnitude higher compared to the inelastic ones at such energies (see, e.g. Ref. [49]). The ionization process will take away the amount of energy corresponding to the adiabatic ionization potential of the target, allene, which is 9.7 eV and the remaining excess energy will be deposited as internal energy for the cations. Considering the electron energy range covered, one could expect that typically only a few of eV (see subsection 2.4 in Ref. [50]) ends up in internal energy of the molecular target. Then, although direct photoionization and electron-impact ionization differ, one can expect a similar trend, supporting the hypothesis of a cyclic product to dominate. According to the energy diagram, this should also hold in the case of propyne.

The formation of less prominent $C_3H_2^+$ is thought to occur directly from the CH_3CCH^+ structure—note that we observed slightly more $C_3H_2^+$ with propyne than with allene. The cyclic isomer of $C_3H_2^+$ is also accessible, possibly without a barrier, but both these channels are not expected to contribute significantly.

The temperature dependence of the branching ratios gives further insights into these two competing CT mechanisms. While it has been shown previously that the near-resonant dissociative CT is largely independent of collision energy,[51] the nondissociative CT mechanism is not. Here, the slight but consistent increase of the yield toward $C_3H_4^+$ with decreasing temperature, associated with nonresonant, nondissociative CT for both target hydrocarbons, simply reflects the greater probability to form a bound complex at low collision energy, even after the long-range CT deposited such internal energy into $C_3H_4^+$. Since the electron transfer processes are mainly driven by nonadiabatic couplings at

long range, a quantitative explanation for this mechanism cannot be provided as the treatment of such complex processes is out of the scope of the present work. However, we can expect that, at lower collision energies, the charge transfer mechanisms lead to $C_3H_4^+$ cations with less internal energy and higher kinetic energy, which can be observed in the mass spectra as well. At higher temperatures, the primary $C_3H_4^+$ cation is formed with more internal energy which may effectively initiate a unimolecular decomposition into smaller species. Respectively, higher branching ratios are expected for the $C_3H_3^+$ and $C_3H_2^+$ products with less amount of $C_3H_4^+$ in this case.

$C_3H_3^+$ in Titan's atmosphere Latest models coupling ion and neutral chemical networks [10,19], supported by Cassini observations, have simulated the vertical density profile of many ionized and neutral organics in Titan's atmosphere. In terms of mole fraction, ionized species concentrate in the ionosphere spanning the 700-1400 km altitude range, where ionic processes play a key part in the chemistry [19] and in the formation of heavy molecules acting as aerosol embryos [52]. The generative or destructive role of ions is however not restricted to charged species and can notably include the production of neutrals, in particular through dissociative recombination. At an altitude of 1000 km, the most abundant hydrocarbons ions are $C_2H_5^+$, $C_3H_3^+$, $C_3H_5^+$ followed by CH_5^+, $C_5H_5^+$ and $C_5H_7^+$ [53]. Among them, the $C_3H_3^+$ ion possesses two isomers, which cannot be observationally distinguished: the most energetically stable aromatic cyclopropenyl cation *c*-$C_3H_3^+$ and the linear propargyl cation *l*-$C_3H_3^+$. The major loss process of ionic aromatic species in Titan's atmosphere is commonly considered to be dissociative recombination. Recent photochemical models [11,48] confirm that (neutral) benzene is mainly generated in the thermosphere by ion chemistry and Loison *et al.* note that the large abundance of C_6H_6 in the upper atmosphere is not the result of efficient formation pathways, but instead is due to the fact that once generated, the aromatic ring is preserved from photodissociation in the upper atmosphere.[19] The major loss process for *c*-$C_3H_3^+$ in Titan's atmosphere was also formally identified as dissociative recombination, leading to the formation of *c*-C_3H_2 or *c*-C_3H [10]. In the work of McEwan et al. [55], the authors pointed to the probable presence *c*-C_3H_2 and encouraged its search. Two years ago, the smallest cyclic hydrocarbon cyclopropenylidene *c*-C_3H_2 was effectively discovered in

Titan by Nixon et al. with the help of the Atacama Large Millimeter/sub-millimeter Array (ALMA) radiotelescope, hence confirming this prediction.[56]

Chemical reactivity of $C_3H_3^+$ The reactivity of the $C_3H_3^+$ cation was investigated in the mid-90's in the laboratory at room temperature by employing a low pressure ICR trap (~10^{-6} mbar) [55,57] and high-pressure SIFT methods (~ mbar) [55,58,59]. The linear isomer of $C_3H_3^+$ appears to be significantly more reactive with hydrocarbons than the cyclic isomer of $C_3H_3^+$, due to a greater efficiency in forming a long-lived intermediate and also because the latter is more energetically stable. At high pressure or when the trapping time is long enough, this intermediate complex can be stabilized faster by collisions leading to larger rate coefficients such for the $C_3H_3^+$ + CD_4, C_2H_2 and C_2H_4 reactions where the ionic adduct have been observed. For instance, the reactions between *l*-$C_3H_3^+$ and several small hydrocarbons of interest for Titan as C_2H_2, C_2H_4, C_3H_4 (allene and propyne) and C_3H_6 were measured with rate coefficients around 10^{-9} cm^3 $molecule^{-1}$ s^{-1} in SIFT or ion trap experiments at room temperature, which is close to the Langevin rate constant. In summary, laboratory works evidenced the low chemical reactivity of the *c*-$C_3H_3^+$ ion, making it a terminal species of the chemical network.

Formation pathways of $C_3H_3^+$ in photochemical models The formation route of this carbocation is not completely secured. Recent photochemical models favor the ion – molecule reactions to form $C_3H_3^+$ because the radiative association of C_3H^+ with H_2 to form $C_3H_3^+$, a process which takes place in the interstellar cloud, presents a very low rate (below or around 10^{-12} cm^3 $molecule^{-1}$ s^{-1}). These ion – molecule reactions mainly lead to the formation of the most stable cyclic *c*-$C_3H_3^+$. In the work of Ali *et al.*, a combination of calculations and experiments leads to the conclusion that under low temperature and pressure conditions of Titan's atmosphere, the hydrocarbon chemistry could play a fundamental role in the synthesis of organic compounds. The CH_3^+ + C_2H_2 or C_2H_4 reactions generate the $C_3H_5^+$ ion which is followed by monomolecular decomposition yielding the cyclopropenyl cation *c*-$C_3H_3^+$ [60]. In others recent models, key ion – molecule reactions involve the three most abundant ions, $C_2H_5^+$, $C_2H_4^+$ and CH_3^+ with a density of above 10 cm^{-3} (420, 120 and 31 cm^{-3} respectively at 1125 km) and neutral acetylene C_2H_2, one of the most abundant hydrocarbons with a peak molar fraction around 3.1×10^{-4} at 1077 km. These bimolecular reactions are:

$C_2H_5^+ + C_2H_2 \rightarrow c\text{-}C_3H_3^+ + CH_4$ (5)

$C_2H_4^+ + C_2H_2 \rightarrow c\text{-}C_3H_3^+ + CH_3$ (6)

$CH_3^+ + C_2H_2 \rightarrow c\text{-}C_3H_3^+ + H_2$ (7)

with rate coefficients (in cm^3 $molecule^{-1}$ s^{-1} units) of 6.84×10^{-11}, 6.47×10^{-10} for the reactions (5) and (6) in the Vuitton *et al.* [10] and Dobrijevic *et al.* [19] models and 2.88×10^{-10} for the reaction (7) in the Vuitton *et al.* work and 1.15×10^{-9} for the global reaction $CH_3^+ + C_2H_2$ in the Dobrijevic *et al.* study. Despite the same molar fraction as C_2H_2, ethylene C_2H_4 (for which the INMS detection cannot be easily distinguished from that of C_2H_2 [15]) is not considered as a possible source of $c\text{-}C_3H_3^+$ through the $C_2H_5^+$, $C_2H_4^+$, $CH_3^+ + C_2H_4$ reactions. Indeed, at the exception of an ICR study of the $C_2H_4^+ + C_2H_4$ reaction for which the $C_3H_3^+$ product has been observed [61], the numerous theoretical and experimental studies all conclude that the $C_2H_4^+ + C_2H_4$ and $C_2H_5^+ + C_2H_4$ reactions do not form the $C_3H_3^+$ product [62]. In contrast, C_2H_4 can react with CH_3^+ to preferentially produce the $c\text{-}C_3H_3^+$ isomer through the monomolecular decomposition of $C_3H_5^+$ but this reaction is not a preferred pathway due to its low rate coefficient (the experimental value obtained by ICR measurements is 9.2×10^{-10} cm^3 $molecule^{-1}$ s^{-1}) and its branching ratio leading to the $C_3H_3^+$ formation (5%) [62]. At last, the fourth most abundant ion $C_2H_3^+$ with a density around 14 cm^{-3} at 1125 km[10], reacting with C_2H_2 or C_2H_4 doesn't form $C_3H_3^+$ [62].

$N_2^+ + C_3H_4$: a new pathway to form $c\text{-}C_3H_3^+$ in Titan's ionosphere? Among all the detected hydrocarbon species, the two isomers of C_3H_4 have been included in several photochemical models [10,18,19,63]. Their total abundance is comparable to C_2H_2 and surpasses the one of the other considered C_3 hydrocarbons. In the coupled ion-neutral photochemical model of Vuitton *et al.* [10], the abundances of propyne $CH_3\text{-}C_2H$ and allene CH_2CCH_2 peak in the upper atmosphere with very similar calculated maximum mole fractions, e.g. of 1.5×10^{-5} and 1.8×10^{-5} cm^{-3} at 1075 km. Their combined contribution (3.3×10^{-5} molecule cm^{-3}) falls in between the uncorrected ($6.31\pm0.24\times10^{-6}$ molecule cm^{-3}) and corrected ($1.4\pm0.9\times10^{-4}$ molecule cm^{-3}) mole fractions from INMS [15,53]. Around the same altitude, from both Dobrijevic et al. [19] and Vuitton et al. [10] photochemical models, the N_2^+ abundance peaks at around 50 cm^{-3} (around 1100 km) for the first model and at 37 cm^{-3} (1125 km) for the second

one which is the same order of magnitude as the CH_3^+ density. The concentration of this primitive photolysis product cannot however be directly established by mass spectrometry because of the overlap with $HCNH^+$ considered to be 40 times more abundant and in a lesser extent with $C_2H_4^+$.

Our work combining laboratory experiments and theoretical considerations (see the energetic landscape of the Figure 7) shows that the reaction of N_2^+ with both C_3H_4 isomers generates dominantly *c*-$C_3H_3^+$ ions over the low temperature range explored (T= 24–71.6 K) and to a lesser extent the $C_3H_2^+$ and $C_3H_4^+$ cations. The nature of the $C_3H_2^+$ isomer remains elusive considering our incomplete understanding of the energetic landscape. However, given the low efficiency of the $C_3H_2^+$ and $C_3H_4^+$ exit channels, their inclusion in the chemical network will affect only marginally the overall chemical setting. The story is not the same for the cyclopropenyl *c*-$C_3H_3^+$ cation. Its reaction enthalpy is lower than that of *l*-$C_3H_3^+$ by 1.19 eV, and these isomers are protected from isomerization with a significant barrier of at least 2.17 eV. [48] In a warmer environment, such as the one characterizing Titan's atmosphere above 800 km in which the gas temperature reaches 150 K, we can reasonably assume that the branching ratio into the *c*-$C_3H_3^+$ channel will be similar. Since the exoergicity is large, the additional energy corresponding to a temperature rise from 70 to 150 K should not allow populating much more levels. The branching ratio into $C_3H_3^+$ measured at 70 K of 0.85 can be then considered as a lower limit. Based on these premises and on the reported channel-specific reaction rate (see above) the reaction of N_2^+ with C_3H_4 isomers may participate in the production of *c*-$C_3H_3^+$.

To evaluate the possible contribution of this pathway to the formation of *c*-$C_3H_3^+$ we included the evaluated reaction rates within a photochemical model of Titan's atmosphere[64] that has been updated with the latest chemical network coupling ion and neutral chemistry from Vuitton *et al.* [10]. Our calculations suggest that the N_2^+ + CH_3C_2H/CH_2CCH_2 contribution has a secondary role compared to the dominant production terms from the reactions of $C_2H_4^+$ and $C_2H_5^+$ with acetylene (Figure 8). At the production peak near 1125 km, the cumulative contribution of the N_2^+ + C_3H_4 channels (dashed black line) is comparable to other secondary production pathways such as from reaction of CH_2^+ with C_2H_2 and CH_3^+ with C_2H_2, C_2H_4 and HC_3N. However, at its maximum contribution the N_2^+ pathway is ~40x

lower than the total production rate (solid black line), while its column integrated contribution is about 2% of the total column production above 600 km.

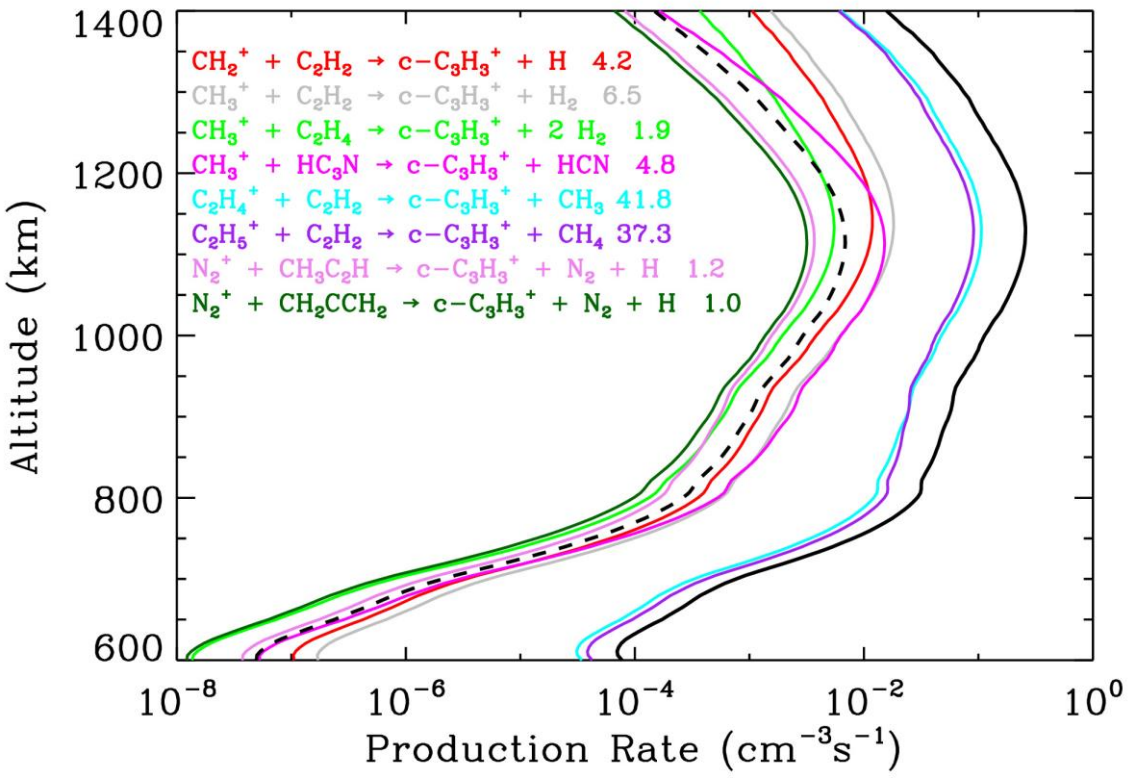

FIG 8: Contribution of different chemical pathways to the production of c-$C_3H_3^+$ in Titan's upper atmosphere. The indicated values represent the percentage contributions of each reaction to the total column production rate above 600 km.

V. CONCLUSION

The rate coefficients and the branching ratios for the reactions of N_2^+ with propyne (CH_3CCH) and allene (CH_2CCH_2) have been experimentally determined at 24, 36, 49 and 72 K using the CRESU-SIS apparatus. All measured rate constants are collisional, agreeing remarkably with capture models. Three primary products $C_3H_2^+$ (*m/z*=38 u), $C_3H_3^+$ (*m/z*=39 u), and $C_3H_4^+$ (*m/z*=40 u) have been clearly identified, the main one being $C_3H_3^+$. The temperature-dependence of the branching ratios between

these three exit channels show a subtle evolution toward more nondissociative charge transfer as the temperature decreases, a trend consistent with the formation of a bound complex occurring after the long-range charge transfer.

Our results, combined with previous work on the unimolecular decomposition of $C_3H_4^+$, show that the reaction of N_2^+ with both isomers of C_3H_4 generates primarily $C_3H_3^+$, plausibly under its cyclic form. The lower reactivity of *c*-$C_3H_3^+$ with linear hydrocarbons compared to its linear *l*-$C_3H_3^+$ form[65] makes the presence of the cyclic isomer likely in Titan's atmosphere. Our evaluation on Titan's atmospheric photochemistry suggests that the contribution of this pathway to the formation of cyclic $C_3H_3^+$ is however of secondary importance relative to other pathways.

This work confirms the potential of our updated experimental approach in providing temperature-dependent branching ratios of ion-molecule reactions. Future experiments will focus on the reactivity of key molecular ions for astrophysical environments such as CH_3^+, whose neutral counterparts are not available off the shelf. Although reaction rates and branching ratios are available for a large selection of ion-molecule reactions, mostly at room temperature, large discrepancies between reported values persist and temperature dependence studies remain rare, especially at low temperatures.

ACKNOWLEDGMENTS

We express our gratitude to the referees for their time and valuable comments, which contributed to improve the quality of the manuscript. We thank J. Courbe for the mechanical design and J. Thiévin for the data acquisition. The implementation of the mass-selective ion source onto the CRESU reactor was funded by the Agence Nationale de la Recherche through the Anion CosChem Project (ANR-14-CE33-0013). We are grateful to Fasmatech for their expert help in ion optics. This work was also supported by the national research programs Physique et Chimie du Milieu Interstellaire (PCMI) and Programme National de Planétologie (PNP) of CNRS/INSU with INC/INP and cofunded by CEA and CNES. We wish to acknowledge the support from the CINES/GENCI for awarding us access to the OCCIGEN supercomputer within the A0070411036 project.

SUPPORTING INFORMATION

The Supporting Information is available free of charge at https://pubs.acs.org/10.1021/acsearthspacechem.1c00347

It contains the calculated relative enthalpies for the product channels of the N_2^+ + CH_3CCH reaction at 0 K as well as the geometries, total electronic and zero-point vibrational energies and harmonic vibrational frequencies of all molecular species, which were studied by means of UCCSD/aug-cc-pVDZ theory.

REFERENCES

(1) Niemann, H. B.; Atreya, S. K.; Bauer, S. J.; Carignan, G. R.; Demick, J. E.; Frost, R. L.; Gautier, D.; Haberman, J. A.; Harpold, D. N.; Hunten, D. M.; Israel, G.; Lunine, J. I.; Kasprzak, W. T.; Owen, T. C.; Paulkovich, M.; Raulin, F.; Raaen, E.; Way, S. H. The Abundances of Constituents of Titan's Atmosphere from the GCMS Instrument on the Huygens Probe. *Nature* **2005**, *438* (7069), 779–784.

(2) Thelen, A. E.; Nixon, C. A.; Chanover, N. J.; Cordiner, M. A.; Molter, E. M.; Teanby, N. A.; Irwin, P. G. J.; Serigano, J.; Charnley, S. B. Abundance Measurements of Titan's Stratospheric HCN, HC_3N, C_3H_4, and CH_3CN from ALMA Observations. *Icarus* **2019**, *319*, 417–432. https://doi.org/10.1016/j.icarus.2018.09.023.

(3) Marten, A.; Hidayat, T.; Biraud, Y.; Moreno, R. New Millimeter Heterodyne Observations of Titan: Vertical Distributions of Nitriles HCN, HC_3N, CH_3CN, and the Isotopic Ratio $^{15}N/^{14}N$ in Its Atmosphere. *Icarus* **2002**, *158* (2), 532–544. https://doi.org/10.1006/icar.2002.6897.

(4) Coustenis, A.; Salama, A.; Schulz, B.; Ott, S.; Lellouch, E.; Encrenaz, T. h; Gautier, D.; Feuchtgruber, H. Titan's Atmosphere from ISO Mid-Infrared Spectroscopy. *Icarus* **2003**, *161* (2), 383–403. https://doi.org/10.1016/S0019-1035(02)00028-3.

(5) Rengel, M.; Sagawa, H.; Hartogh, P.; Lellouch, E.; Feuchtgruber, H.; Moreno, R.; Jarchow, C.; Courtin, R.; Cernicharo, J.; Lara, L. M. Herschel/PACS Spectroscopy of Trace Gases of the Stratosphere of Titan. *A&A* **2014**, *561*, A4. https://doi.org/10.1051/0004-6361/201321945.

(6) Coustenis, A.; Achterberg, R. K.; Conrath, B. J.; Jennings, D. E.; Marten, A.; Gautier, D.; Nixon, C. A.; Flasar, F. M.; Teanby, N. A.; Bézard, B.; Samuelson, R. E.; Carlson, R. C.; Lellouch, E.; Bjoraker, G. L.; Romani, P. N.; Taylor, F. W.; Irwin, P. G. J.; Fouchet, T.; Hubert, A.; Orton, G. S.; Kunde, V. G.; Vinatier, S.; Mondellini, J.; Abbas, M. M.; Courtin, R. The Composition of Titan's Stratosphere from Cassini/CIRS Mid-Infrared Spectra. *Icarus* **2007**, *189* (1), 35–62. https://doi.org/10.1016/j.icarus.2006.12.022.

(7) Maltagliati, L.; Bézard, B.; Vinatier, S.; Hedman, M. M.; Lellouch, E.; Nicholson, P. D.; Sotin, C.; de Kok, R. J.; Sicardy, B. Titan's Atmosphere as Observed by Cassini/VIMS Solar Occultations: CH_4, CO and Evidence for C_2H_6 Absorption. *Icarus* **2015**, *248*, 1–24. https://doi.org/10.1016/j.icarus.2014.10.004.

(8) Koskinen, T. T.; Yelle, R. V.; Snowden, D. S.; Lavvas, P.; Sandel, B. R.; Capalbo, F. J.; Benilan, Y.; West, R. A. The Mesosphere and Lower Thermosphere of Titan Revealed by Cassini/UVIS Stellar Occultations. *Icarus* **2011**, *216* (2), 507–534. https://doi.org/10.1016/j.icarus.2011.09.022.

(9) Waite, J. H.; Niemann, H.; Yelle, R. V.; Kasprzak, W. T.; Cravens, T. E.; Luhmann, J. G.; McNutt, R. L.; Ip, W.-H.; Gell, D.; De La Haye, V.; Müller-Wordag, I.; Magee, B.; Borggren, N.; Ledvina, S.; Fletcher, G.; Walter, E.; Miller, R.; Scherer, S.; Thorpe, R.; Xu, J.; Block, B.;

Arnett, K. Ion Neutral Mass Spectrometer Results from the First Flyby of Titan. *Science* **2005**, *308* (5724), 982–986. https://doi.org/10.1126/science.1110652.
(10) Vuitton, V.; Yelle, R. V; Klippenstein, S. J.; Hörst, S. M.; Lavvas, P. Simulating the Density of Organic Species in the Atmosphere of Titan with a Coupled Ion-Neutral Photochemical Model. *Icarus* **2019**, *324*, 120–197. https://doi.org/10.1016/j.icarus.2018.06.013.
(11) McEwan, M. J.; Anicich, V. G. Titan's Ion Chemistry: A Laboratory Perspective. *Mass Spectrometry Reviews* **2007**, *26* (2), 281–319. https://doi.org/10.1002/mas.20117.
(12) Dutuit, O.; Carrasco, N.; Thissen, R.; Vuitton, V.; Alcaraz, C.; Pernot, P.; Balucani, N.; Casavecchia, P.; Canosa, A.; Picard, S. L.; Loison, J.-C.; Herman, Z.; Zabka, J.; Ascenzi, D.; Tosi, P.; Franceschi, P.; Price, S. D.; Lavvas, P. Critical Review of N, N^+, N_2^+, N^{++}, and N_2^{++} Main Production Processes and Reactions of Relevance to Titan's Atmosphere. *ApJS* **2013**, *204* (2), 20. https://doi.org/10.1088/0067-0049/204/2/20.
(13) Maguire, W. C.; Hanel, R. A.; Jennings, D. E.; Kunde, V. G.; Samuelson, R. E. C_3H_8 and C_3H_4 in Titan's Atmosphere. *Nature* **1981**, *292* (5825), 683–686. https://doi.org/10.1038/292683a0.
(14) Magee, B. A.; Waite, J. H.; Mandt, K. E.; Westlake, J.; Bell, J.; Gell, D. A. INMS-Derived Composition of Titan's Upper Atmosphere: Analysis Methods and Model Comparison. *Planetary and Space Science* **2009**, *57* (14), 1895–1916. https://doi.org/10.1016/j.pss.2009.06.016.
(15) Cui, J.; Yelle, R. V.; Vuitton, V.; Waite, J. H.; Kasprzak, W. T.; Gell, D. A.; Niemann, H. B.; Müller-Wodarg, I. C. F.; Borggren, N.; Fletcher, G. G.; Patrick, E. L.; Raaen, E.; Magee, B. A. Analysis of Titan's Neutral Upper Atmosphere from Cassini Ion Neutral Mass Spectrometer Measurements. *Icarus* **2009**, *200* (2), 581–615. https://doi.org/10.1016/j.icarus.2008.12.005.
(16) Vinatier, S.; Bézard, B.; Nixon, C. A.; Mamoutkine, A.; Carlson, R. C.; Jennings, D. E.; Guandique, E. A.; Teanby, N. A.; Bjoraker, G. L.; Michael Flasar, F.; Kunde, V. G. Analysis of Cassini/CIRS Limb Spectra of Titan Acquired during the Nominal Mission: I. Hydrocarbons, Nitriles and CO_2 Vertical Mixing Ratio Profiles. *Icarus* **2010**, *205* (2), 559–570. https://doi.org/10.1016/j.icarus.2009.08.013.
(17) Lombardo, N. A.; Nixon, C. A.; Greathouse, T. K.; Bézard, B.; Jolly, A.; Vinatier, S.; Teanby, N. A.; Richter, M. J.; G Irwin, P. J.; Coustenis, A.; Flasar, F. M. Detection of Propadiene on Titan. *ApJ* **2019**, *881* (2), L33. https://doi.org/10.3847/2041-8213/ab3860.
(18) Li, C.; Zhang, X.; Gao, P.; Yung, Y. Vertical Distribution of C_3-Hydrocarbons in the Stratosphere of Titan. *ApJ* **2015**, *803* (2), L19. https://doi.org/10.1088/2041-8205/803/2/L19.
(19) Dobrijevic, M.; Loison, J. C.; Hickson, K. M.; Gronoff, G. 1D-Coupled Photochemical Model of Neutrals, Cations and Anions in the Atmosphere of Titan. *Icarus* **2016**, *268*, 313–339. https://doi.org/10.1016/j.icarus.2015.12.045.
(20) Abeysekera, C.; Joalland, B.; Ariyasingha, N.; Zack, L. N.; Sims, I. R.; Field, R. W.; Suits, A. G. Product Branching in the Low Temperature Reaction of CN with Propyne by Chirped-Pulse Microwave Spectroscopy in a Uniform Supersonic Flow. *J. Phys. Chem. Lett.* **2015**, *6* (9), 1599–1604. https://doi.org/10.1021/acs.jpclett.5b00519.
(21) Gerlich, D. Ion-Neutral Collisions in a 22-Pole Trap at Very Low Energies. *Physica Scripta* **1995**, *1995* (T59), 256.
(22) Wester, R. Radiofrequency Multipole Traps: Tools for Spectroscopy and Dynamics of Cold Molecular Ions. *J. Phys. B: At. Mol. Opt. Phys.* **2009**, *42* (15), 154001. https://doi.org/10.1088/0953-4075/42/15/154001.
(23) Biennier, L.; Carles, S.; Cordier, D.; Guillemin, J.-C.; Le Picard, S. D.; Faure, A. Low Temperature Reaction Kinetics of CN^-+HC_3N and Implications for the Growth of Anions in Titan's Atmosphere. *Icarus* **2014**, *227*, 123–131. https://doi.org/10.1016/j.icarus.2013.09.004.
(24) Bourgalais, J.; Jamal-Eddine, N.; Joalland, B.; Capron, M.; Balaganesh, M.; Guillemin, J.-C.; Le Picard, S. D.; Faure, A.; Carles, S.; Biennier, L. Elusive Anion Growth in Titan's Atmosphere: Low Temperature Kinetics of the C_3N^- + HC_3N Reaction. *Icarus* **2016**, *271*, 194–201. https://doi.org/10.1016/j.icarus.2016.02.003.
(25) Joalland, B.; Jamal-Eddine, N.; Kłos, J.; Lique, F.; Trolez, Y.; Guillemin, J.-C.; Carles, S.; Biennier, L. Low-Temperature Reactivity of C2n+1N– Anions with Polar Molecules. *J. Phys. Chem. Lett.* **2016**, *7* (15), 2957–2961. https://doi.org/10.1021/acs.jpclett.6b01191.

(26) Biennier, L.; Carles, S.; Lique, F.; Mitchell, J. B. Ion Chemistry in Uniform Supersonic Flows. In *Uniform Supersonic Flows in Chemical Physics: Chemistry studied using the CRESU method close to Absolute Zero, B.R. Rowe, A. Canosa, D.E. Heard (Eds.)*; 2021.
(27) Joalland, B.; Jamal-Eddine, N.; Papanastasiou, D.; Lekkas, A.; Carles, S.; Biennier, L. A Mass-Selective Ion Transfer Line Coupled with a Uniform Supersonic Flow for Studying Ion–Molecule Reactions at Low Temperatures. *J. Chem. Phys.* **2019**, *150* (16), 164201. https://doi.org/10.1063/1.5086386.
(28) Kato, S.; Bierbaum, V. M.; Leone, S. R. Multiquantum Vibrational Deactivation of N_2^+(v) by Collisions with N_2 and O_2 at Thermal Energies. *J. Phys. Chem. A* **1998**, *102* (33), 6659–6667. https://doi.org/10.1021/jp981679k.
(29) Ferguson, E. E. Vibrational Quenching of Small Molecular Ions in Neutral Collisions. *J. Phys. Chem.* **1986**, *90* (5), 731–738. https://doi.org/10.1021/j100277a008.
(30) Wilson, P. F.; Freeman, C. G.; McEwan, M. J. Reactions of Small Hydrocarbons with H_3O^+, O_2^+ and NO^+ Ions. *International Journal of Mass Spectrometry* **2003**, *229* (3), 143–149. https://doi.org/10.1016/S1387-3806(03)00290-2.
(31) Milligan, D. B.; Wilson, P. F.; Freeman, C. G.; Meot-Ner, M.; McEwan, M. J. Dissociative Proton Transfer Reactions of H_3^+, N_2H^+, and H_3O^+ with Acyclic, Cyclic, and Aromatic Hydrocarbons and Nitrogen Compounds, and Astrochemical Implications. *J. Phys. Chem. A* **2002**, *106* (42), 9745–9755. https://doi.org/10.1021/jp014659i.
(32) *NIST Chemistry WebBook, NIST Standard Reference Database Number 69*; Linstrom, P. J., Mallard, W. G., Eds.; National Institute of Standards and Technology: Gaithersburg MD, 20899, 2005.
(33) KIDA. KInetic Database for Astrochemistry http://kida.obs.u-bordeaux1.fr/.
(34) Decker, B. K.; Adams, N. G.; Babcock, L. M. Gas-Phase Reactivity of $SO^{+}\cdot$: A Selected Ion Flow Tube Study11Dedicated to the Memory of Robert R. Squires. *International Journal of Mass Spectrometry* **2000**, *195–196*, 185–201. https://doi.org/10.1016/S1387-3806(99)00146-3.
(35) Werner, H. J.; Knowles, P. J.; Knizia, G.; Manby, F. R.; Schütz, M.; Celani, P.; Györffy, W.; Kats, D.; Korona, T.; Lindh, R. MOLPRO, Version 2015.1, a Package of Ab Initio Programs. *University of Cardiff Chemistry Consultants (UC3): Cardiff, Wales, UK* **2015**.
(36) Werner, H. J.; Knowles, P. J.; Knizia, G.; Manby, F. R.; Schütz, M. WIREs Comput. Mol. Sci. 2, 242–253 (2012). *version* **2012**.
(37) Gray, C. G.; Gubbins, K. E. *Theory of Molecular Fluids. Volume 1: Fundamentals*; Clarendon Press: Oxford, 1984.
(38) Su, T.; Chesnavich, W. J. Parametrization of the Ion–Polar Molecule Collision Rate Constant by Trajectory Calculations. *The Journal of Chemical Physics* **1982**, *76* (10), 5183–5185. https://doi.org/10.1063/1.442828.
(39) Rankin, D. W. H. CRC Handbook of Chemistry and Physics, 89th Edition, Edited by David R. Lide. *null* **2009**, *15* (3), 223–224. https://doi.org/10.1080/08893110902764125.
(40) Gussoni, M.; Rui, M.; Zerbi, G. Electronic and Relaxation Contribution to Linear Molecular Polarizability. An Analysis of the Experimental Values. *Journal of Molecular Structure* **1998**, *447* (3), 163–215. https://doi.org/10.1016/S0022-2860(97)00292-5.
(41) Tsuji, M.; Kouno, H.; Matsumura, K.; Funatsu, T.; Nishimura, Y.; Obase, H.; Kugishima, H.; Yoshida, K. Dissociative Charge-transfer Reactions of Ar^+ with Simple Aliphatic Hydrocarbons at Thermal Energy. *The Journal of Chemical Physics* **1993**, *98* (3), 2011–2022. https://doi.org/10.1063/1.464234.
(42) Gichuhi, W. K.; Suits, A. G. Primary Branching Ratios for the Low-Temperature Reaction of State-Prepared N_2^+ with CH_4, C_2H_2, and C_2H_4. *J. Phys. Chem. A* **2011**, *115* (25), 7105–7111. https://doi.org/10.1021/jp112427r.
(43) Mebel, A. M.; Bandrauk, A. D. Theoretical Study of Unimolecular Decomposition of Allene Cations. *J. Chem. Phys.* **2008**, *129* (22), 224311. https://doi.org/10.1063/1.3037204.
(44) Parr, A. C.; Jason, A. J.; Stockbauer, R. Photoionization and Threshold Photoelectron-Photoion Coincidence Study of Allene from Onset to 20 EV. *International Journal of Mass Spectrometry and Ion Physics* **1978**, *26* (1), 23–38. https://doi.org/10.1016/0020-7381(78)80002-3.
(45) Parr, A. C.; Jason, A. J.; Stockbauer, R.; McCulloh, K. E. Photoionization and Threshold Photoelectron—Photoion Coincidence Study of Propyne from Onset to 20 eV. *International*

Journal of Mass Spectrometry and Ion Physics **1979**, *30* (3), 319–330. https://doi.org/10.1016/0020-7381(79)83009-0.
(46) Ho, G. H.; Lin, M. S.; Wang, Y. L.; Chang, T. W. Photoabsorption and Photoionization of Propyne. *J. Chem. Phys.* **1998**, *109* (14), 5868–5879. https://doi.org/10.1063/1.477209.
(47) Liu, G.; Li, Z.; Ding, Y.; Fu, Q.; Huang, X.; Sun, C.; Tang, A. Water-Assisted Isomerization from Linear Propargylium (H2CCCH+) to Cyclopropenylium (c-$C_3H_3^+$). *J. Phys. Chem. A* **2002**, *106* (43), 10415–10422. https://doi.org/10.1021/jp0212085.
(48) Marimuthu, A. N.; Sundelin, D.; Thorwirth, S.; Redlich, B.; Geppert, W. D.; Brünken, S. Laboratory Gas-Phase Vibrational Spectra of $[C_3H_3]^+$ Isomers and Isotopologues by IRPD Spectroscopy. *Journal of Molecular Spectroscopy* **2020**, *374*, 111377. https://doi.org/10.1016/j.jms.2020.111377.
(49) Możejko, P.; Ptasińska-Denga, E.; Domaracka, A.; Szmytkowski, C. Absolute Total Cross-Section Measurements for Electron Collisions with Tetrahydrofuran. *Phys. Rev. A* **2006**, *74* (1), 012708. https://doi.org/10.1103/PhysRevA.74.012708.
(50) Gross, J. H. Principles of Ionization and Ion Dissociation. In *Mass Spectrometry: A Textbook*; Gross, J. H., Ed.; Springer International Publishing: Cham, 2017; pp 29–84. https://doi.org/10.1007/978-3-319-54398-7_2.
(51) Masson, A. J.; Birkinshaw, K.; Henchman, M. J. Collision Mechanism of a Dissociative Charge-Transfer Reaction at Low Energy. *J. Chem. Phys.* **1969**, *50* (9), 4112–4114. https://doi.org/10.1063/1.1671676.
(52) Lavvas, P.; Yelle, R. V.; Koskinen, T.; Bazin, A.; Vuitton, V.; Vigren, E.; Galand, M.; Wellbrock, A.; Coates, A. J.; Wahlund, J.-E.; Crary, F. J.; Snowden, D. Aerosol Growth in Titan's Ionosphere. *Proc. Natl. Acad. Sci. U.S.A.* **2013**, *110* (8), 2729–2734. https://doi.org/10.1073/pnas.1217059110.
(53) Waite, J. H., Jr.; Young, D. T.; Cravens, T. E.; Coates, A. J.; Crary, F. J.; Magee, B.; Westlake, J. The Process of Tholin Formation in Titan's Upper Atmosphere. *Science* **2007**, *316* (5826), 870–875. https://doi.org/10.1126/science.1139727.
(54) Loison, J. C.; Dobrijevic, M.; Hickson, K. M. The Photochemical Production of Aromatics in the Atmosphere of Titan. *Icarus* **2019**, *329*, 55–71. https://doi.org/10.1016/j.icarus.2019.03.024.
(55) McEwan, M. J.; McConnell, C. L.; Freeman, C. G.; Anicich, V. G. Reactions of Isomeric $C_3H_3^+$ Ions: A Combined Low Pressure-High Pressure Study. *J. Phys. Chem.* **1994**, *98* (19), 5068–5073. https://doi.org/10.1021/j100070a021.
(56) Nixon, C. A.; Thelen, A. E.; Cordiner, M. A.; Kisiel, Z.; Charnley, S. B.; Molter, E. M.; Serigano, J.; Irwin, P. G. J.; Teanby, N. A.; Kuan, Y.-J. Detection of Cyclopropenylidene on Titan with ALMA. *AJ* **2020**, *160* (5), 205. https://doi.org/10.3847/1538-3881/abb679.
(57) Smyth, K. C.; Lias, S. G.; Ausloos, P. The Ion-Molecule Chemistry of $C_3H_3^+$ and the Implications for Soot Formation. *Combustion Science and Technology* **1982**, *28* (3–4), 147–154. https://doi.org/10.1080/00102208208952550.
(58) Prodnuk, S. D.; Grocert, S.; Bierbaum, V. M.; DePuy, C. H. Gas-Phase Reactions of $C_3H_n^+$ Ions. *Organic Mass Spectrometry* **1992**, *27* (4), 416–422. https://doi.org/10.1002/oms.1210270411.
(59) Smith, D.; Adams, N. G. Cyclic and Linear Isomers of $C_3H_2^+$ and $C_3H_3^+$: The $C_3H^+ + H_2$ Reaction. *International Journal of Mass Spectrometry and Ion Processes* **1987**, *76* (3), 307–317. https://doi.org/10.1016/0168-1176(87)83035-5.
(60) Ali, A.; Sittler, E. C.; Chornay, D.; Rowe, B. R.; Puzzarini, C. Organic Chemistry in Titan's Upper Atmosphere and Its Astrobiological Consequences: I. Views towards Cassini Plasma Spectrometer (CAPS) and Ion Neutral Mass Spectrometer (INMS) Experiments in Space. *Planetary and Space Science* **2015**, *109–110*, 46–63. https://doi.org/10.1016/j.pss.2015.01.015.
(61) O'Malley, R. M.; Jennings, K. R. Ion Cyclotron Resonance Mass Spectra of Fluoroalkenes I. Ion—Molecule Reactions of Ethylene and Vinyl Fluoride. *International Journal of Mass Spectrometry and Ion Physics* **1969**, *2* (6), 441–455. https://doi.org/10.1016/0020-7381(69)80042-2.
(62) Anicich, V. G. An Index of the Literature for Bimolecular Gas Phase Cation-Molecule Reaction Kinetics. *JPL Publication 03-19* **2003**, *1–1194*.

(63) Hébrard, E.; Dobrijevic, M.; Loison, J. C.; Bergeat, A.; Hickson, K. M.; Caralp, F. Photochemistry of C_3H_p Hydrocarbons in Titan's Stratosphere Revisited. *A&A* **2013**, *552*, A132. https://doi.org/10.1051/0004-6361/201220686.
(64) Lavvas, P. P.; Coustenis, A.; Vardavas, I. M. Coupling Photochemistry with Haze Formation in Titan's Atmosphere, Part I: Model Description. *Planetary and Space Science* **2008**, *56* (1), 27–66. https://doi.org/10.1016/j.pss.2007.05.026.
(65) Ausloos, P.; Lias, S. G. Discrimination of $C_3H_3^+$ Structures on the Basis of Chemical Reactivity. *J. Am. Chem. Soc.* **1981**, *103* (21), 6505–6507. https://doi.org/10.1021/ja00411a045.